The Journal of Experimental Biology 211, 1859-1867
Published by The Company of Biologists 2008
doi:10.1242/jeb.014134

Hydrodynamic performance of the minke whale (*Balaenoptera acutorostrata*) flipper

Lisa Noelle Cooper[1,2,*], Nils Sedano[3], Stig Johansson[4], Bryan May[5], Joey D. Brown[6], Casey M. Holliday[7], Brian W. Kot[8] and Frank E. Fish[9]

[1]Department of Anatomy, Northeastern Ohio Universities College of Medicine, Rootstown, OH 44201, USA, [2]School of Biomedical Sciences, Kent State University, Kent, OH 44242, USA, [3]Air Force Research Laboratory, Liquid Rocket Engines Branch, 4 Draco Drive, Edwards Air Force Base, CA 93524, USA, [4]Department of Aerospace Engineering and Engineering Mechanics, San Diego State University, 5500 Campanile Drive, San Diego, CA 92182, USA, [5]2217 Burrough Street, Unit #1, San Diego, CA 92111, USA, [6]NASA Jet Propulsion Laboratory, 4800 Oak Grove Drive M/S T1723-118, Pasadena, CA 91109, USA, [7]Department of Anatomy and Pathology, Joan C. Edwards School of Medicine, 1542 Spring Valley Drive, Huntington, WV 25704, USA, [8]Department of Ecology and Evolutionary Biology, University of California, Los Angeles, Box 1606, 621 Charles E. Young Drive South, Los Angeles, CA 90095-1606, USA and [9]Department of Biology, West Chester University, 750 S. Church Street, West Chester, PA 19383, USA

*Author for correspondence (e-mail: l.noelle.cooper@gmail.com)

Accepted 1 April 2008

SUMMARY

Minke whales (*Balaenoptera acutorostrata*) are the smallest member of balaenopterid whales and little is known of their kinematics during feeding maneuvers. These whales have narrow and elongated flippers that are small relative to body size compared to related species such as right and gray whales. No experimental studies have addressed the hydrodynamic properties of minke whale flippers and their functional role during feeding maneuvers. This study integrated wind tunnel, locomotion and anatomical range of motion data to identify functional parameters of the cambered minke whale flipper. A full-sized cast of a minke whale flipper was used in wind tunnel testing of lift, drag and stall behavior at six speeds, corresponding to swimming speeds of 0.7–8.9 m s^{-1}. Flow over the model surface stalled between 10° and 14° angle of attack (α) depending on testing speed. When the leading edge was rotated ventrally, loss in lift occurred around –18° α regardless of speed. Range of mobility in the fresh limb was approximately 40% greater than the range of positive lift-generating angles of attack predicted by wind tunnel data (+14° α). Video footage, photographs and observations of swimming, engulfment feeding and gulping minke whales showed limb positions corresponding to low drag in wind tunnel tests, and were therefore hydrodynamically efficient. Flippers play an important role in orienting the body during feeding maneuvers as they maintain trim of the body, an action that counters drag-induced torque of the body during water and prey intake.

Key words: Cetacea, forelimb, flipper, wind tunnel, hydrodynamics, feeding, control surface, engulfment, lunge.

INTRODUCTION

Cetaceans (whales, dolphins and porpoises) are exceptional mammals that have adapted to life in a marine environment. They are the only marine mammals that have achieved fast swimming speeds, while also obtaining some of the largest mammalian body sizes in evolutionary history. The two modern suborders, Odontoceti (toothed whales) and Mysticeti (baleen whales), display a variety of adaptations that aid in an aquatic lifestyle, such as hindlimb and hair loss, streamlined and fusiform body contours, and blowholes on the top on their heads. Cetaceans have also evolved four control surfaces that effect rotation about each axis during locomotion – flukes, caudal peduncles, dorsal fins and pectoral flippers (Fish, 2002; Fish, 2004). Cetacean pectoral flippers are composed of the bony elements plesiomorphic to those of tetrapods (humerus, radius, ulna, carpals, metacarpals and digits), all encased in dense connective tissues, creating a stiffened flipper (Fig. 1). Flippers, once deployed, manipulate flow around the body by altering angle of attack and sweep angle to aid in steering, but do not oscillate and do not generate propulsion or thrust during rectilinear locomotion.

Compared to other aquatic vertebrates, cetaceans differ either in the structure or function of the pectoral limb. Fish use pectoral fins and other control surfaces to generate thrust and balancing forces (Drucker and Lauder, 1999; Lauder and Drucker, 2004; Fish and Lauder, 2006) by actively controlling fin curvature, displacement and fin area *via* contractions of muscles that insert on the rays embedded within the fins (Lauder, 2005; Fish and Lauder, 2006). Shark pectoral fins are stiff, but function to alter body pitch *via* changes in the fin trailing edge (Lauder and Drucker, 2004). Cetacean flippers are stiffened as in sharks, but unlike sharks and rays, retain several bones within the flipper, manipulate flow *via* coordinated contraction of muscles housed mostly within the body wall, and little deformation has been reported in the flippers in most cetaceans (Cooper et al., 2007b).

Role of the cetacean flipper during feeding

Balaenopterid whales, including minke whales, employ engulfment feeding, in which a whale will approach a patch of aggregated prey at a high speed and engulf thousands of liters of water and prey, causing an enlarged ventral throat pouch to distend (Lambertsen et al., 1995; Goldbogen et al., 2006, 2007). While the mouth closes, water is pushed through the baleen (Lambertsen et al., 1995), forcing prey to be captured by fringes of baleen along the lingual sides of baleen plates. Although the function of the balaenopterid feeding apparatus has been the subject of anatomical (e.g. Lambertsen et

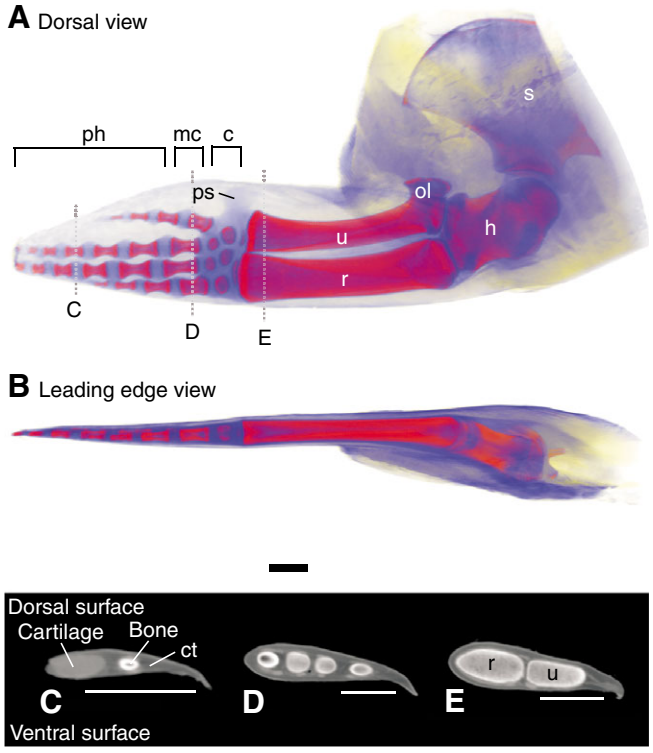

Fig. 1. Minke whale (*Balaenoptera acutorostrata*) flipper in (A) dorsal view and (B) leading edge view. Bones colored red, cartilage colored blue. Dotted lines indicate planes of section. (C–E) Flipper cross-sections along the (C) distal end of the flipper, (D) metacarpals and (E) distal radius and ulna. The cambered nature of the flipper is shown in D and E as the ventral surface of the flipper is more convex than the dorsal surface. The tapered trailing edge of the flipper was partially deformed during packaging for CT scanning, but normally would be in line with the chord axis. c, carpals; ct, dense connective tissue; h, humerus; mc, metacarpals; ol, olecranon process of the ulna; ph, phalanges; ps, cartilaginous anlage of the pisiform bone; r, radius; s, scapula; u, ulna. Scale bar, 5 cm.

al., 1995; Lambertsen and Hintz, 2004) and experimental (e.g. Goldbogen et al., 2006) studies, no experiments have tested flipper function associated with gulping and engulfment feeding behaviors. This study aims to expand understanding of the hydrodynamic performance of the flipper and its role during feeding maneuvers.

Studies addressing the functional role of the balaenopterid forelimb have either hypothesized the function based on anatomical observations (e.g. Howell, 1930; Benke, 1993; Fish and Battle, 1995; Woodward et al., 2006), or placed synthetic models of flippers in wind tunnels to explore the behavior of air over the surface of the model (Miklosovic et al., 2004). No tests in water have been conducted.

This study integrates anatomical, observational and experimental data to report on the hydrodynamic performance of the cambered minke whale (*Balaenoptera acutorostrata* Lacépède 1804) flipper, and addresses the functional role of the flipper during feeding maneuvers. A cast of a fresh minke whale flipper was constructed and used for wind tunnel testing of lift, drag and stall behavior. Objectives of this study were to identify the functional range of the minke whale forelimb, angles and speed at which the model stalls, and optimal angles of attack for hydrodynamic efficiency. These data were then integrated to address the hydrodynamic performance of the minke whale flipper during engulfment maneuvers.

MATERIALS AND METHODS

Anatomical observations

To determine the range of motion at the glenohumeral joint, a fresh neonatal minke whale limb (*Balaenoptera acutorostrata*, COA no. 020717Ba; Fig. 1) with an attached scapula, obtained from the College of the Atlantic (COA) in Bar Harbor, ME, USA, was rotated through its full range of motion. The scapula was secured with clamps, and range of positive angles of attack (α) was determined through manipulation of the flipper to the most extreme possible angle. Digital images and videos documented this range of motion. No data were gathered regarding negative angles of attack as the laboratory architecture did not allow the scapula to be secured while manipulating the limb in negative angles of attack.

Three dimensional architecture of the limb was observed both *via* computed axial tomography (CT) scans and anatomical dissection. The entire flipper was scanned using a GE Light Plus CT Scanner. CT images of the flipper were then compiled and visualized with Amira 4.1 (Mercury Computer Systems, Carlsbad, CA, USA; Fig. 1). Detailed osteological and soft tissue descriptions of this flipper are published elsewhere (Cooper et al., 2007a; Cooper et al., 2007b).

Locomotion observations

Observations of dwarf minke whale locomotion were based on the television documentary 'Mystery of the Minkes' (Natural History New Zealand, 2002) and photos (Arnold et al., 2005), which showed exceptional footage of the dwarf minke whale swimming and engaging in non-feeding gulping behavior. Furthermore, observations of surface-lunge feeding maneuvers supplemented these data (Kot, 2005). Although it was not possible to reliably gather quantitative data on forelimb position and range of motion, qualitative data of forelimb position during swimming, gliding and gulping behaviors were gathered. Also, based on still photos of engulfing and feeding balaenopterid whales, further insight was added to standard orientations of flippers during different engulfing maneuvers.

Wind tunnel experiments

A mold and cast (Fig. 2) were made of the flipper of a fresh neonatal stranded specimen of minke whale (*Balaenoptera acutorostrata*, COA no. 020717Ba; Fig. 1). The rubber mold of the flipper was made by wrapping the fresh limb in thin plastic and using a mixture of RTV silicone and accelerator. A hard mother mold was made using plaster (Silicast casting urethane; Silpak, Pomona, CA, USA) and Hydrocal FGR-95 gypsum cement with 10 mm thick monofilament fiberglass. The flipper cast was then created by filling the mold with plaster casting urethane (Fig. 2). Before the urethane dried, a metal rod was embedded along the longitudinal axis for attachment to the yaw plate of the wind tunnel (Fig. 2). Remnants of skin folds in the axillary region of the cast were sanded and then smoothed with aluminium tape. The model had a maximum thickness of 6.5 cm, tip thickness of 0.3 cm, and total length of 70 cm (Fig. 2). The average model thickness was 3.5 cm, with an average chord length of 18.0 cm (Fig. 2).

The flipper model was biologically realistic in shape in comparison to the fresh flipper (Figs 1, 2, *B. acutorostrata*, COA no. 020717Ba), but differed in its mechanical properties. The model was rigid along its entire length, whereas the fresh flipper had some flexibility in the digits (Cooper et al., 2007b), and the trailing edge of the fresh flipper had a thin layer of skin that probably deformed with water flow.

Fig. 2. Minke whale (*Balaenoptera acutorostrata*) flipper model, cast from a fresh flipper. After removal of skin folds from the model, aluminium tape was used to smooth the base of the model. This model was used for wind tunnel testing of lift, drag and stall behaviors. (A) Dorsal view, (B) ventral view. Scale bar, 10 cm.

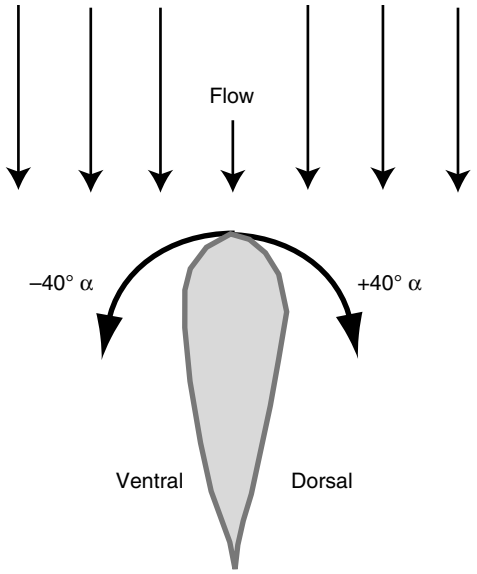

Fig. 3. Orientation of the flipper model in the wind tunnel as seen from above. Data were collected every 2° as the model was rotated between +40 and –40 angle of attack (α).

Wind tunnel tests were performed in the low speed, single return, closed jet, continuous flow wind tunnel at the San Diego State University, Department of Aerospace Engineering and Engineering Mechanics. Airflow was generated by a 150HP electric motor driving a variable pitched, four-blade propeller. The test section was 1149 mm wide, 819 mm high and 1727 mm long. The model was mounted on a computer-controlled turntable with a 0.01 degree resolution.

To match swimming speeds and wind tunnel speeds, two Reynolds number equations were used: one equation with values specific for air flow behavior, and a second with values for sea water flow behavior. Experiments were conducted at a range of Reynolds numbers (Table 1; Re=1.7×10^5–5.9×10^5), using the equation Re=(ρlU)/μ, where ρ refers to fluid density (ρ_{air}=1.29 kg m^{-3}), l is the length of the object in the direction of flow, in this case the chord length (0.129 m), U is the swimming speed (m s^{-1}), and μ is the dynamic viscosity (Ns m^{-2}) (Reynolds, 1883; Vogel, 1994).

Wind tunnel tests were conducted with the model mounted vertically, perpendicular to flow, which is consistent with the flipper orientation of a minke whale while engulfing, i.e. the leading edge orientation is perpendicular to flow (Fig. 3) (Arnold et al., 2005). The model was rotated from –40 to +40° α, in two degree increments yielding a total of 40 angle measurements at each testing speed (Fig. 3). A cruising minke whale has been observed with a speed of 3.25 m s^{-1} (Blix and Folkow, 1995). A total of six wind tunnel speeds/whale swimming speeds were examined during our experiments (Table 1): 17.4 m s^{-1}/0.7 m s^{-1} (N=3, Re=171 002), 25.9 m s^{-1}/1.7 m s^{-1} (N=3, Re=254 100), 30.4 m s^{-1}/2.3 m s^{-1} (N=2, Re=298 249), 34.4 m s^{-1}/2.9 m s^{-1} (N=3, Re=337 492), 45.6 m s^{-1}/5.1 m s^{-1} (N=4, Re=447 373), and 60.4 m s^{-1}/8.9 m s^{-1} (N=3, Re=592 574). This testing range both exceeds and falls well below reported swimming speed.

As with standard aero/hydrodynamic measurements, the flipper cast was positioned with its base against the flat base of the wind tunnel (Miklosovic et al., 2004), which is functionally analogous

Table 1. Flow behavior over the surface of the flipper model during all speed trials

Wind tunnel speed (m s^{-1})	Stall angle (°)		Maximum C_L	Angle of max. C_L (°)	Minimum C_D	Angle of min. C_D (°)	Reynolds nos (air)	Swimming speed (m s^{-1})
17.4	+12°	–18*	1.62	+12°	0.02	+2 to +4	171002	0.7
25.9	+10°	–20*	1.55	+10°	0.04	+2	254100	1.7
30.4	+10°	–20*	1.50	+10°	–0.014	+4	298249	2.3
34.4	+10°	–20*	1.48	+10°	0.04	+2	337492	2.9
45.6	+8°	–20*	1.41	+14°	0.04	+2	447373	5.1
60.4	+6°	–18*	1.27	+14°	0.06	0 to +2	592574	8.9

C_L, coefficient of lift; C_D, coefficient of drag.
*Partial stall.

to a wall. This configuration approximated the junction between the flipper and the body of the whale which has a relatively low curvature at the base chord of the flipper (Stewart and Leatherwood, 1985). As the mid-chord of the flipper base was located at approximately 0.26 of body length from the rostrum tip (Stewart and Leatherwood, 1985), drag due to the interference between the body and flipper was comparatively small (Hoerner, 1965). Interference drag is at a maximum when a wing is located at the largest diameter of a fuselage, but is lowest toward the nose. The lift produced by a wing on a fuselage has a slightly higher lift than a wing alone, although a wing canted at an angle would exhibit a slightly lower lift (Hoerner and Borst, 1985). Lift and drag were measured for the minke whale flipper at various angles of attack and therefore provided a reasonable approximation for the actual forces on the flipper, and are consistent with previous wind tunnel experiments based on cetacean flipper models (Miklosovic et al., 2004).

Force and moment data, from the mounted flipper model in the wind tunnel, were gathered through a six-component, load cell, strain-gauge type balance system. The signals from the strain gauges in the balance, which typically produce in the order of 4.5 mV N^{-1}, were amplified using Pacific Model 8655 transducer conditioning amplifiers. These amplifiers, which utilize a low-pass filter with a cut-off frequency of 10 Hz, were set to a gain of 200. Extensive calibration of the balance system demonstrated negligible interaction between the six components (lift, drag, and side force, yaw, pitch and roll) for single axis loadings up to the load limits. Interaction was less than 1% under any combination of loading up to 75% of the load limits. The amplified and filtered signals were then routed to, and acquired in, a standard personal computer equipped with a LabView AT-MIO-16E-2 data acquisition board. A LabView VI (virtual instrument) program, written especially for the San Diego State University low speed wind tunnel, converted the strain gauge signals to engineering units and stored them for subsequent analysis.

Drag and lift values depend on the object's size and speed relative to the fluid's viscosity and density (Vogel, 1994). Therefore, lift (L) and drag (D) values were expressed as dimensionless coefficients [coefficient of lift, $C_L=(2L)/(\rho A_p U^2)$ and coefficient of drag, $C_D=(2D)/(\rho A_s U^2)$ where A_p is the planar surface area of a flipper, and A_s is the total area of a flipper] that are a function of the Reynolds number (Reynolds, 1883; Vogel, 1994).

To visualize flow, tufts (air stream indicators) were attached *via* smoothed aluminium tape to both the dorsal and ventral surfaces of the model. Tufts allow identification of laminar or linear flow along the boundary layer, turbulent flow along the boundary layer, and complete boundary layer separation from the surface of the model. Visual identification the model orientations at which the boundary layer separates was essential as it indicated when flow interacts with outer flow, and is creating a broader wake and increasing drag (Fish and Lauder, 2006). During turbulent flow, the boundary layer is still attached to the surface of the model but is not linear. Complete boundary layer separation occurs when air around the surface of the model is shedding vortices. Digital photos and video recordings were used to examine the flow behavior over the surface of the model at various combinations of speed and angles of attack.

Resulting lift and drag data were then used in a full-body model of a minke whale to estimate the magnitude of forces created by the flippers *versus* those created by the body during engulfment maneuvers. Based on illustrations from Stewart and Leatherwood (Stewart and Leatherwood, 1985), the center of mass of a minke whale was located at 46% of the body length, and the flippers were located well anterior to this at approximately 27% of the body length (4.8 m). The drag created by an open mouth was positioned at the centroid of the triangular lower jaw in frontal view, and was calculated from the equation, $\text{Drag}=0.5\rho A C_d U^2$, where ρ is the density of sea water, A is the frontal area of the lower jaw (0.376 m^2), C_d is the drag coefficient, based on a hollow half sphere (Vogel, 1994), and U was the swimming speed of 2.3 m s^{-1}. The drag torque was calculated as the product of the drag, lever arm (2.2 m; dashed blue line; distance from the point of application of the drag to the center of mass), and sine of the angle between the lever arm and horizontal line. The lift produced by the flippers was calculated from the equation, $\text{Lift}=0.5\rho A_f C_l V^2$, where A_f is the combined planar area of the flippers (0.184 m^2) and C_l is the maximum lift coefficient (1.5). The lift torque was calculated as the produce of the lift and the lever arm (1.3 m; distance from flippers to center of mass).

RESULTS

Anatomical observations

The fresh flipper (*B. acutorostrata*, COA no. 020717Ba) was secured in the same orientation as used in the wind tunnel tests (Fig. 3) and rotated from 0° to +27° α during passive manipulation in which only the angles of attack were altered. Detailed anatomical descriptions of this specimen are published elsewhere (Cooper et al., 2007a; Cooper et al., 2007b).

Results of the three-dimensional (3D) visualization of the minke whale flipper (*B. acutorostrata*, COA no. 020717Ba) are shown in Fig. 1. These data show the flipper forms a hydrofoil with a rounded leading edge and a tapered trailing edge (Fig. 1C–E). The flipper is dorsoventrally flattened (Fig. 1B), and rather than displaying symmetry, each of the flipper cross sections illustrate the cambered nature of the flipper (Fig. 1C–E).

This elongated flipper is supported throughout its length by both cartilaginous and bony elements. The flipper protrudes out of the body wall at the level of the mid-humerus, and the leading edge is supported by an elongated radius and ulna that compose approximately 45% of the flipper length (Fig. 1A,B,E). The wrist consists of five bony carpal elements immersed in cartilage, and together these structures make up 9% of the flipper length (Fig. 1A). Along the trailing edge of the wrist is the cartilaginous anlage of the pisiform bone, which creates a trailing edge extension of the wrist (Fig. 1A). Both the metacarpals and phalanges are arranged into four digital rays that with cartilaginous joints that account for 41% of the total flipper length (Fig. 1A). The radius and ulna and the metacarpals and phalanges therefore account for approximately equal amounts of the flipper length. Rather than being broad and paddle-like, the flipper is narrow, with the greatest chord lengths corresponding to two trailing edge extensions of the flipper, the olecranon process of the ulna, and the pisiform cartilage of the wrist (Fig. 1A). The three digital rays closest to the leading edge are closely appressed with little interdigital space (Fig. 1A,D), and the radius, located nearest the leading edge, appears to be of a larger diameter than the caudally placed ulna (Fig. 1A,E).

Locomotion observations

Observations of flipper movements in swimming minke whales showed flippers were typically held in one of three general positions. During vertical ascents and descents, the flipper was typically held flush to the body wall, thus increasing the streamlined nature of the body by reducing drag. While swimming, or cruising, the minke whales held their flippers swept back at approximately 45° and near zero angles of attack. During non-feeding gulping maneuvers, the

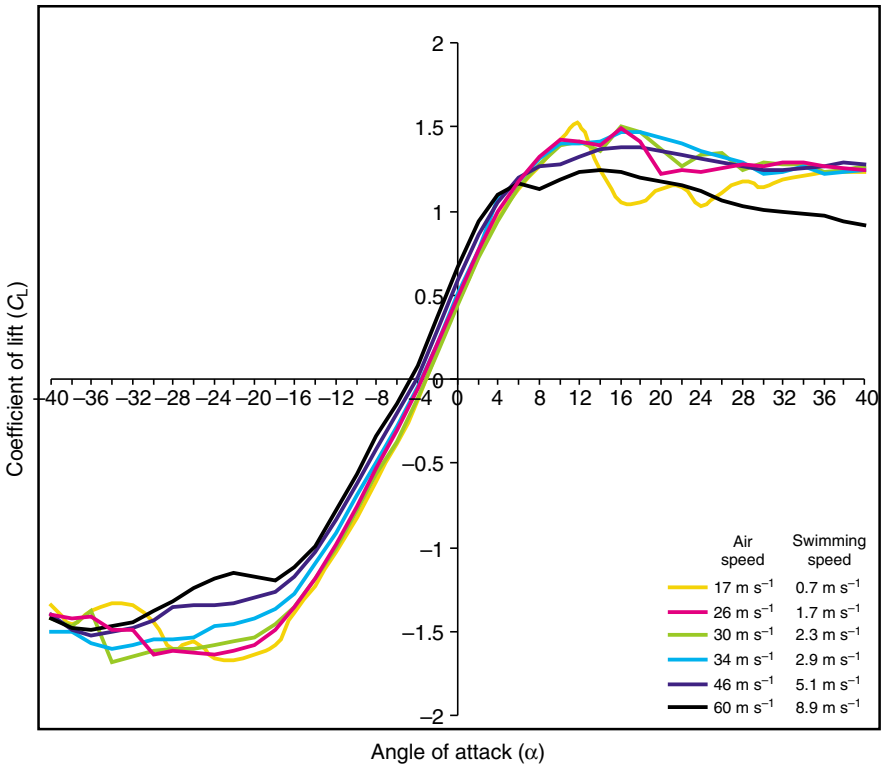

Fig. 4. Averaged lift data for the minke whale flipper model. Averaged wind tunnel measurements of the lift coefficient, C_L, shown as a function of the angle of attack, α, on the *x*-axis at 17 m s^{-1} (yellow), 26 m s^{-1} (pink), 30 m s^{-1} (green), 34 m s^{-1} (light blue), 46 m s^{-1} (indigo) and 60 m s^{-1} (black).

flipper was held perpendicular to the longitudinal axis of the body, with a sweep angle near zero (Arnold et al., 2005), and with angles of attack near 0°. During gulps, the body moved forward *via* propulsion from the tail, and as the mouth opened, the rostrum was raised (Arnold et al., 2005). The flippers were then rotated forward to approximately 0° sweep, and 0° α. While the mouth was closing, flippers were returned to the swept-back position associated with cruising and sometimes held flush against the body wall.

Wind tunnel experiments

Coefficient of lift (C_L) data were gathered as a function of angle of attack (α) for each testing speed and these raw data were then averaged and plotted as the average C_L *vs* α (Fig. 4), and reported in Table 1. A near linear relationship was found between C_L and α for a total range of 32° α at the slowest speed (17 m s^{-1}) and 26° at the highest speeds (46 and 60 m s^{-1}; Fig. 4). This near linear slope of 0.11 for all speeds indicated flow was attached to the model surface, and stall did not occur during those flow states (Fig. 4). The *y*-intercept (α=0) of all trials occurred between approximately 0.4 and 0.6 C_L (Fig. 4).

A substantial loss in lift indicates flow separation, or stall, along a large part of the surface of the model. While testing in the range of positive α (raising the leading edge of the model) at 17 m s^{-1}, a drop in C_L occurred most dramatically at +12° α, with a 31% drop in C_L (Fig. 4, Table 1). During the 26, 30 and 34 m s^{-1} trials, between +12° and +14° α, there was a slight drop in C_L (1% drop), and at +16° α, the C_L reached a maximum at 1.49 (Fig. 4, Table 1). At α greater than +16°, C_L declined, indicating a separation of the boundary layer over the dorsal surface of the model (Fig. 4, Table 1). The 45.6 m s^{-1} trial showed an initial slight loss of C_L at 8° (Fig. 4, Table 1). This initial loss in lift was followed by a plateau until +14° α where the lift gradually declined. The 60 m s^{-1} trial indicated an initial drop in C_L from 6–8° α. At 12° α, the C_L was constant until 16° α, and then gradually declined (Fig. 4, Table 1).

Contrary to the more abrupt losses in lift in the positive angles of attack, all loss of lift along the negative angles of attack was gradual up to –25° α (Fig. 4). Beginning at –18° α, testing speeds of 26–60 m s^{-1} showed a similar value of C_L (Fig. 4). Different experimental speeds could be distinguished by their differing C_L levels at each plateau with 17 m s^{-1} having the lowest C_L (–1.6; Fig. 4) and 60 m s^{-1} displaying the value closest to positive C_L (–1.2; Fig. 4). Within the negative α range, data indicated distinct C_L values for 26, 30 and 34 m s^{-1}. At 26 m s^{-1}, the negative tail of the curve reached a plateau at approximately –1.6 C_L, compared to –1.56 for 30 m s^{-1}, and –1.4 for 34 m s^{-1} (Fig. 4).

In all speed trials, there was a steady increase in drag at angles of α further away from 0°, and the lowest drag was found at low positive angles of attack (Fig. 5). The angles for which the drag was lowest indicates the flipper orientations that would be most hydrodynamically efficient at generating lift. The lowest drag was found usually in a four degree range for each tested speed, between 0° and +4° α (Fig. 5, Tables 1 and 2). However at speeds of 60 m s^{-1}, a narrower window of low drag was found between 0° and +2° α. At 17 m s^{-1} the least amount of drag was found between +2° and +4° α (C_D=0.02). The least amount of drag, at 26 m s^{-1}, was found between +2° (C_D=0.04) and +4° α (C_D=0.05; Fig. 5, Table 1).

Table 2. Range of coefficient of lift and coefficient of drag values and associated standard error of the estimates (s.e.e.) for all testing speeds at angles of attack corresponding to the least amount of drag

Angle of attack (α)	Lift (C_L range)	s.e.e. (lift)	Drag (C_D range)	s.e.e. (drag)
0	0.45–0.66	0.01–0.22	–0.01–0.06	0.003–0.07
2	0.73–0.94	0.04–0.14	–0.01–0.08	0.003–0.08
4	0.94–1.10	0.02–0.15	–0.0008–0.12	0.003–0.09

C_L, coefficient of lift; C_D, coefficient of drag.

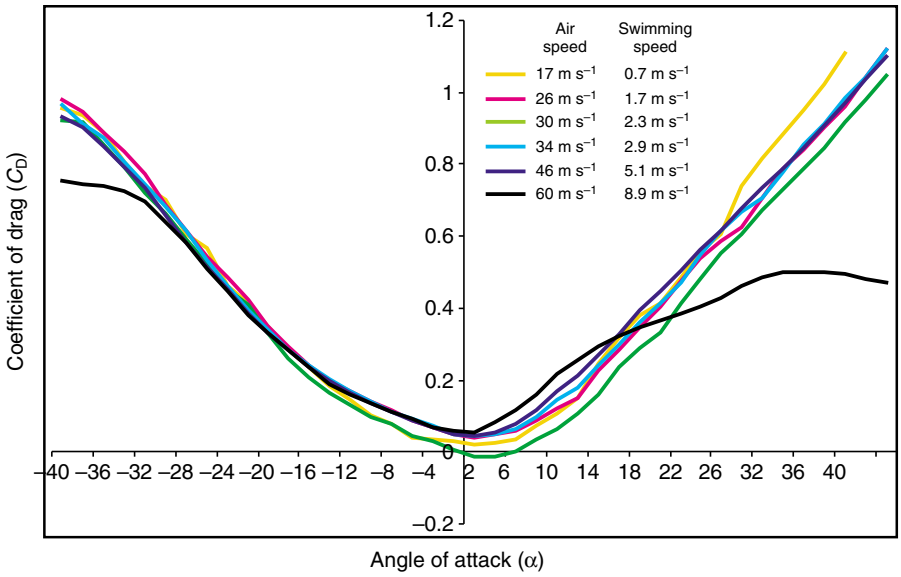

Fig. 5. Averaged drag data for the minke whale flipper model. Averaged wind tunnel measurements of the drag coefficient, C_D, shown as a function of the angle of attack, α, on the *x*-axis at 17 m s^{-1} (yellow), 26 m s^{-1} (pink), 30 m s^{-1} (green), 34 m s^{-1} (light blue), 46 m s^{-1} (indigo) and 60 m s^{-1} (black).

Compared to other data, the minimum C_D range at 30 m s^{-1} was noted at a larger α, and displayed the lowest values at +2° α (C_D=–0.01) and +6° α (C_D=–0.001). Both 34 m s^{-1} and 46 m s^{-1} showed a C_D minimum of 0.04 at +2° α. The minimum range of the average C_D was the most narrow for the 60 m s^{-1} trial, and spanned only two degrees [0° α (C_D=0.059) to +2° α (C_D=0.056); Fig. 5, Table 1]. Ratios of C_L to C_D were calculated and the higher the ratio, the more theoretically efficient the flipper would be at generating lift, and the more efficient the limb orientation would be for cruising. Data indicate the greatest efficiency at 0° α at 26 m s^{-1} (C_L:C_D of 641), +2° α at 34.4 m s^{-1} (C_L:C_D of 381), and +6° α at 26 m s^{-1} (C_L:C_D of 148). The inflated ratio value at 0° α, is a result of drag values near zero. Negative drag values are theoretically impossible as this would imply the flipper was being sucked forward, and these values may have been caused by the tip of the model being close to the wind tunnel boundaries, thus creating interference in the model and wind tunnel boundary layers.

Tufts placed along both the dorsal and ventral surfaces of the model identified areas of laminar and turbulent boundary layer flow and complete separation of the boundary layer over the surface of the model (Fig. 6). Laminar flow was found along most of both surfaces of the model at 17 m s^{-1}, +10° α (Fig. 6A), as indicated by the near linear slope of the C_L in the wind tunnel data (Fig. 4). At positive angles of attack beyond the near linear slope range of C_L, turbulent flow or complete separation should occur mostly on the dorsal surface of the model. Tufts placed along the dorsal surface of the model showed that flow separation began first along the trailing edge of the flipper, and then spread to the base and tip, and finally the entire dorsal surface indicating stall (Fig. 6A–D). At positive angles of attack, an ideal flipper model should retain laminar

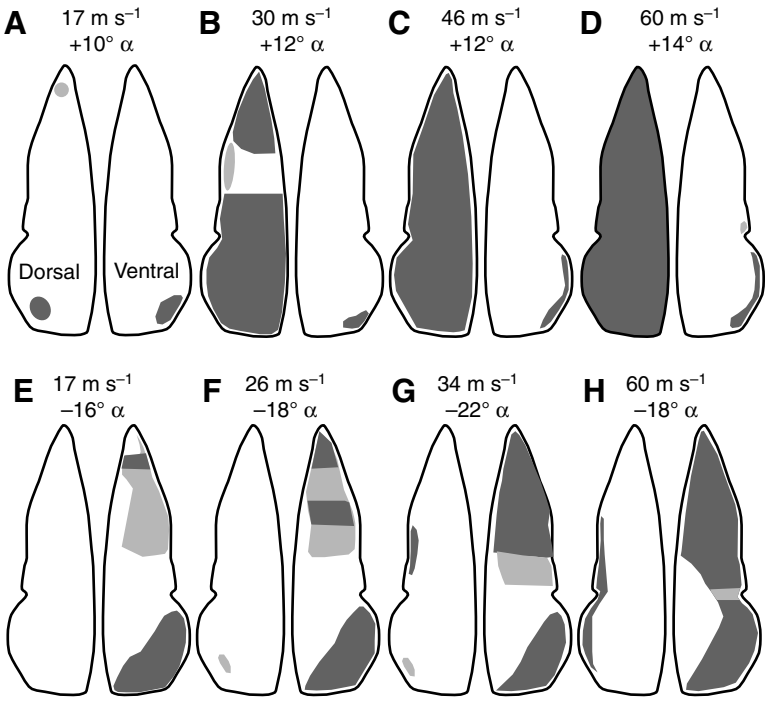

Fig. 6. Air flow behavior over the model based on movements of tufts (air stream indicators) attached to the surface of the model during wind tunnel testing. The model is outlined in black, with areas of laminar flow in white, turbulent flow in gray and complete boundary layer separation in black. (A) Flow behavior at +10° α at 17 m s^{-1}, (B) +12° α at 30 m s^{-1}, (C) +12° α at 46 m s^{-1}, (D) +14° α at 60 m s^{-1}, (E) –16° α at 17 m s^{-1}, (F) –18° α at 26 m s^{-1}, (G) –22° α at 34 m s^{-1} and (H) –18° α at 60 m s^{-1}.

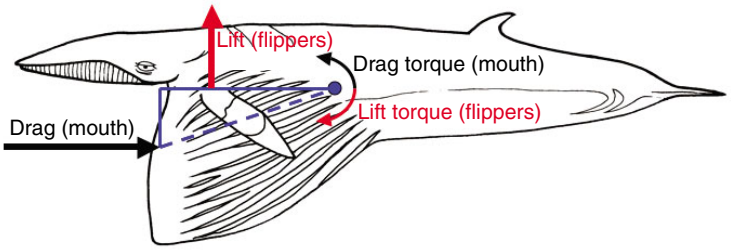

Fig. 7. Model of forces (drag, lift) resulting in the development of torque to stabilize a feeding minke whale. The features shown are: the center of mass of the whale (blue circle); drag (straight black arrow) from the open mouth, which is positioned at the centroid of triangular lower jaw in frontal view; drag torque (curved black arrow); drag lever arm (dashed blue line); and lift torque (curved red arrow). The lift torque was found to be slightly larger than the drag torque created by the open mouth.

flow over the entire ventral surface of the model. However in the axillary region, near the ventral surface base, a small pocket of flow separation was found along the trailing edge of the model at low speeds (17 m s^{-1} and 30 m s^{-1}; Fig. 6A,B). At higher speeds, flow separation occurred along the trailing edge of most the model (46 m s^{-1} and 60 m s^{-1}; Fig. 6C,D).

In an ideal model, turbulent and separated flow would be restricted to the ventral surface of the model at negative angles of attack. However, in the axillary region, at the base of the dorsal surface, a small pocket of turbulent flow was found along the trailing edge of the model beginning at 26 m s^{-1} (Fig. 6E) and this pocket enlarged and flow became more unstable until complete separation was found along the trailing edge of most of the base at higher speeds (60 m s^{-1}; Fig. 6H). Along the ventral surface of the model, flow was separated along the tip and base (axillary region), turbulent near the middle of the model, and laminar along a wide swath in the middle near the leading edge, at 17 m s^{-1} and 26 m s^{-1} (Fig. 6E,F). At higher speeds (34 and 60 m s^{-1}), flow never completely separated over the ventral surface as the leading edge portion near the middle of the model maintained laminar flow (Fig. 6G,H). In total, tufts indicated that at negative angles of attack flow along the ventral surface did not completely separate and therefore complete stall was not observed.

Modeling drag and lift forces on a feeding minke whale indicate that the lift torque generated by the flippers was slightly larger than the drag torque created by the open mouth (Fig. 7). The lift and lift coefficient of the flippers were found to be 747.0 N and 1.5, whereas the drag and drag coefficient of the lower jaw were 1449.1 N and 1.42. Similarly, the torque of the flippers (N m) was found to be 664.9 N m, whereas the torque of the lower jaw was found to be 579.8 N m.

DISCUSSION

The flipper as a hydrofoil

The cetacean forelimb is shaped like a hydrofoil in that it is dorsoventrally flattened with a rounded leading edge and tapered trailing edge (Fig. 1C–E). Hydrodynamic pressures concentrate along this leading edge, which is supported by bony structures that add structural integrity to the flipper (Fig. 1A).

Besides the cross-sectional dimensions of the flipper, three other characteristics are essential for creating a limb that acts as a hydrofoil: the flipper needs to be long, stiff and webbed. Elongation increases area that will manipulate flow around the body, and is achieved by increasing the number of bones in the limb and changing limb allometry. Most mammals have retained or reduced the plesiomorphic phalangeal count of 2/3/3/3/3, but cetaceans are the only mammals that have increased the number of phalanges, a morphology termed hyperphalangy (Fig. 1A,B) (for a review, see Howell, 1930). By evolving hyperphalangy, cetaceans change limb allometry by increasing manus length relative to limb length. Minke whale digital rays account for about 40% of the flipper length (Fig. 1A,B), whereas in some dolphins (i.e. Risso's dolphin) the digital rays account for 65% of flipper length. Some mysticetes have also elongated the radius and ulna (Fig. 1A,B), which can account for approximately half of the flipper length (45% of the flipper length in the minke whale), but most odontocetes have reduced the length of these bones.

Cetaceans reduced flipper deformation by evolving several stiffening structures throughout the limb. Alterations to joint structure have greatly reduced skeletal mobility throughout the limb. The elbow (or cubital) joint is immobilized as bony constraints lock the joint, and the wrist is mostly immobilized by closely appressed carpal elements that lack the ability to glide relative to another (Fig. 1A). Surrounding the digits is a thick and dense layer of connective tissue that minimizes movements of the digits, and this connective tissue continues along the length of the flipper to stiffen the wrist, and support the radius and ulna (Fig. 1). In some cases, the connective tissue layer alone is thicker than the digits. By increasing limb stiffness, the flipper functions as a hydrofoil in which flow is manipulated by active contractions of limb musculature, but passive movements of the limb do not effect flow (Fish and Lauder, 2006). This flipper stiffness is in strong contrast to the highly flexible fins of some fish. Fish fins do not act as hydrofoils as they readily deform due to both active contractions of the fin musculature and deformations caused by fluid loads (Fish and Lauder, 2006).

Unlike most mammals, cetaceans do not have digits that are anatomically separate from one another – they are webbed together in a single flipper (Fig. 1). By retaining tissues between the digits, a smooth contour is created along the chord of the flipper (the distance between the leading and trailing edges; Fig. 1). This smooth contour facilitates laminar flow and boundary layer adhesion to the surface of the flipper, and is therefore essential for lift generation.

The flipper is simply deployed as a stiff hydrofoil, rather than being used as an oscillator to generate propulsion. The magnitude of lift and drag forces on a given wing or flipper are affected by the spanwise and radial flow pressure differences at the tip and those vortices that are being shed at the tip (Ellington et al., 1996; Birch and Dickinson, 2001; Bandyopadhyay et al., 2008). For flapping motions, such as in the case of the wings of insects and the pectoral fins of some fishes, the spanwise flow helps to stabilize flow over the lifting surface and maintain lift in unsteady conditions. In contrast to this, the flippers of minke whales, when extended perpendicular to the longitudinal axis of the body, would experience a comparatively steadier flow and less spanwise flow. Indeed, the tapered planform shape of the flippers would limit pressure differences at the flipper tip and decrease the magnitude of tip vortices, which are associated with induced drag. van Dam (van Dam, 1987) showed that a tapered wing planform with crescent cross-sectional shape could reduce the induced drag by 8.8% compared to a wing with an elliptical planform. Minimal induced drag is fostered by a swept wing planform with a root chord (proximal chord) greater than the chord at the tips giving a

triangular shape (Küchermann, 1953; Ashenberg and Weihs, 1984). This optimal shape approximates the planform of the minke whale flipper.

Taken together, it appears that the cetacean flipper is a complex structure in which several skeletal and soft tissue structures create a hydrofoil-shaped limb that is capable of generating lift and acting as a control surface to manipulate fluid flow around the body.

Efficacy of the model

Data gathered from wind tunnel testing of lift and drag parameters, and stall behavior provided insight into the efficacy of the minke whale flipper model. A total of six wind tunnel speeds/whale swimming speeds were examined during our experiments (Table 1): 17.4 m s^{-1}/0.7 m s^{-1} (N=3, Re=171002), 25.9 m s^{-1}/1.7 m s^{-1} (N=3, Re=254100), 30.4 m s^{-1}/2.3 m s^{-1} (N=2, Re=298249), 34.4 m s^{-1}/2.9 m s^{-1} (N=3, Re=337492), 45.6 m s^{-1}/5.1 m s^{-1} (N=4, Re=447373) and 60.4 m s^{-1}/8.9 m s^{-1} (N=3, Re=592574). Stall, or the point in which the boundary layer along the surface of the model sheds vortices, was abrupt at +12° α at 17 m s^{-1} (Fig. 4). However, only partial stall was observed at high positive angles of attack for the middle testing speeds (26, 30 and 34 m s^{-1}) because laminar flow was retained in the middle of the flipper dorsal surface (Figs 4, 6). At higher speeds (46 and 60 m s^{-1}) flow visualization showed the entire dorsal surface of the model had complete separation of the boundary layer (Fig. 6C,D), indicating complete stall. Contrary to this visual identification of stall (Fig. 6C,D), averaged data from the wind tunnel measurements indicated only a slight loss in lift over a broad range of α, suggesting incomplete flow separation (Fig. 4). At negative angles of attack, the ventral surface failed to have complete flow separation, and therefore only reached partial stall (Fig. 6E–H). Near –18° α for all tested speeds, similar C_L values were maintained over a broad range of angles of attack (Fig. 4) rather than a consistent loss of lift with decreasing angles of attack. In this case, the observed tuft behavior (Fig. 6A–H) was consistent with measured flow behavior suggested by coefficient of lift parameters (Fig. 4).

A possible explanation for the variation between flow data and observations could be that unexpected turbulent flow along the model surfaces obscured accurate readings. Because of this discrepancy, flow visualization was considered essential for accurately interpreting air flow behaviors suggested by the wind tunnel data, and also served as a means to hypothesize possible sources of measurement error. Visualizations (Fig. 6) showed that patches of turbulent flow were found on surfaces that would ideally have been completely laminar. The cast was made from a swept back, fresh and articulated flipper and scapula and to retain the full length of the leading edge, the axillary region had to be reconstructed, and this area of the model consistently shed vortices (Fig. 6E–G). Therefore, the axillary reconstruction may have caused perturbations in the data, but those discrepancies were isolated to the axillary region.

This is the first study to employ a biologically real cast of a flipper, rather than an idealized or known aerodynamic model. Although some perturbations were found in flow over the axillary region, flow over the model predicted general hydrodynamic principles (e.g. stall angles, lift-generating angles) that can be used to address the performance of the minke whale flipper. In an ideal study, replicas of actual flippers could be made based on three dimensional scans, but until these studies are undertaken, this study furthers our understanding of a flipper with a shape like that of an actual balaenopterid flipper.

Performance of the minke whale flipper

Results of the wind tunnel data taken together with locomotion observations and tests of the range of motion provide a broad picture of the possible functional attributes of the minke whale flipper. Unlike other marine mammals that oscillate their flippers to generate propulsion [e.g. pinnipeds, otariids (for a review, see Fish, 2002)], mysticetes deploy flippers into one of three general positions (swept back, flush to the body wall and perpendicular to flow) and alter the angle of the flippers from their stationary positions.

Balaenopterids engulf large amounts of water while feeding, creating a net downward body torque. If this torque was not counteracted, the anterior aspect of the body would pitch downward (ventrally). Whales counteract drag induced by the engorged ventral pouch by several mechanisms. First, locomotion data indicated one or both of the flippers was extended during ventral pouch expansion. Extended flippers were held at low angles of attack, near 0°, which is a hydrodynamically efficient posture corresponding to greatest lift and least drag values (Figs 4, 5). Second, during pouch expansion and forward motion, the palate was raised (Arnold et al., 2005) and experienced dorsally and posteriorly directed forces that probably counteracted body torque. Third, flukes generate both thrust and lift as whales accelerate into prey aggregations, and are probably the most effective at countering body torque. Lastly, some whales arched the vertebral column such that the caudal half of the body was relatively straight but the cranial third of the body was raised to an angle of 15° (Arnold et al., 2005), which would also counteract drag-induced torque. However, field observations show that engulfment can sometimes occur without this spinal movement. By altering flipper and palate orientations, fluking, and sometimes arching the spine, whales are probably able to maintain a positive body pitch, which would facilitate the engulfment of water in the ventral pouch. These data are significant, as feeding in minke whales requires the integration of multiple body parts (i.e. feeding apparatus, body and palate orientation and flipper position) in order to maintain body position during feeding maneuvers. Previous studies have not hypothesized the functional role of the flipper during these behaviors.

Although minke whales may prefer to hold flippers at low angles of attack during engulfment maneuvers, manipulation of a fresh limb indicated a +27° α range of motion. However, experimental results indicated the lift-generating angles of attack between –18° and +12° α, and outside of this range drag exceeded lift (Figs 4, 5). Drag also plays an important role in flipper function. Bottlenose dolphins (*Tursiops truncatus*) slowed forward motion by pronating both flippers and generating drag (Bloodworth and Marshall, 2005). If flippers are asymmetrically oriented, the body will turn in the direction of the flipper creating the greatest drag. Surface feeding minke whales extend one flipper perpendicular to flow while the other is held flush against the body wall, creating a ‘pirouette’ behavior. Therefore, besides generating lift, cetaceans also orient flippers to induce drag and slow forward motion and steer.

By comparing lift, drag and torque forces in a feeding minke whale model, results indicated that even the seemingly tiny flippers of a minke whale generated a slightly larger torque than the drag torque created by an open mouth (Fig. 7). These data imply that deployment of the flippers to a position extended perpendicular to body flow may in fact generate enough lift to counteract drag induced by the open mouth, and that the flippers can function to stabilize body position during feeding maneuvers.

Results of this analysis can be compared to a previous study of a generalized whale flipper, and an idealized humpback whale

(*Megaptera novaeangliae*) flipper. A NACA 0200 airfoil with known aerodynamic parameters, with a shape superficially similar to the minke whale flipper model tested here, stalled near +12° α for testing speeds from 17–34 m s^{-1} (Miklosovic et al., 2004), which was consistent with the results of this study. A NACA 0200 with a scalloped leading edge simulated leading edge tubercles in humpback whales (Fish and Battle, 1995; Miklosovic et al., 2004). The scalloped flipper exhibited a 40% increase in the angle of stall compared to both the NACA 0200 and the minke whale model. Humpback whale flippers appear to be more hydrodynamically efficient at generating and maintaining lift.

Minke whales are the smallest balaenopterid mysticetes with body proportions similar to all nine species of non-humpback balaenopterids (Horwood, 1990). Minke whale flippers are similar in shape and dimensions to all non-humpback balaenopterids, and can be considered representative of the standard balaenopterid flipper. Flippers of other balaenopterid taxa may display similar hydrodynamic properties and stall behaviors.

CONCLUSION

Few studies have documented the orientation of the balaenopterid forelimb during feeding and associated maneuvers. This study integrated experimentally generated hydrodynamic data with observational data to address flipper function in the minke whale. Data indicate the flipper has a range of motion greater than the predicted lift-generating angles of attack. Observations of locomotion behavior indicated the flipper was typically held at angles of attack near 0°, and perpendicular to flow during gulping and feeding maneuvers. Data from this study suggests this flipper orientation is hydrodynamically efficient as it incurs the least amount of drag, but generates a high degree of lift, and this flipper-generated lift force contributes to the increase in pitch of the engulfing whales. Furthermore, our data suggest that the flippers generate sufficient lift torque to counteract the drag torque generated by the open mouth during feeding maneuvers. Taken together, data indicate that the small, narrow flippers of minke whales are control surfaces that play an important role in maintaining a positively-pitched body orientation during various types of feeding maneuvers.

We thank two anonymous reviewers for comments that greatly improved this manuscript. Funding for this project came from an ONR grant number N00014-02-1-0046 to Dr Frank E. Fish. We are greatly appreciative of Dr Joseph Katz for use of the wind tunnel, Dr J. Allen at the College of the Atlantic in Bar Harbor, ME for the fresh minke whale specimen, the late Mr Fritz Clark for assistance in building the flipper model, and Dr Ted Cranford for assistance in obtaining CT scans. We thank Ms Caroline Fyler for assistance with the fresh specimen. We thank Dr Hans Thewissen, Dr Chris Vinyard, Mr Ronald B. Cooper, Mr Tobin L. Hieronymus, Ms Megan F. McKenna and Ms Angela Horner for helpful comments on this manuscript. We thank Mr Zach Mellor and Mrs Liliana Fajardo-Mellor for discussions, Mr Cory M. Redman and Mr Kesler A. Randall for logistical assistance, and Mr Victor Sanchez for data collection assistance.

REFERENCES

Arnold, P. W., Birtles, R. A., Sobtzick, S., Matthews, M. and Dunstan, A. (2005). Gulping behavior in rorqual whales: underwater observations and functional interpretation. *Mem. Queensl. Mus.* **51**, 309-332.

Ashenberg, J. and Weihs, D. (1984). Minimum induced drag of wings with curved planform. *J. Aircr.* **21**, 89-91.

Bandyopadhyay, P. R., Beal, D. N. and Menozzi, A. (2008). Biorobotic insights into how animals swim. *J. Exp. Biol.* **211**, 206-214.

Benke, H. (1993). Investigations on the osteology and the functional morphology of the flipper of whales and dolphins (Cetacea). *Invest. Cetacea* **24**, 9-252.

Birch, J. M. and Dickenson, M. H. (2001). Spanwise flow and the attachment of the leading-edge vortex on insect wings. *Nature* **412**, 729-733.

Blix, A. S. and Folkow, L. (1995). Daily energy requirements in free living minke whales. *Acta Physiol. Scand.* **153**, 61-66.

Bloodworth, B. and Marshall, C. D. (2005). Feeding kinematics of Kogia and Tursiops (Odontoceti:Cetacea): characterization of suction and ram feeding. *J. Exp. Biol.* **208**, 3721-3730.

Cooper, L. N., Berta, A., Dawson, S. D. and Reidenberg, J. S. (2007a). Evolution of hyperphalangy and digit reduction in the cetacean manus. *Anat. Rec. Hoboken* **209**, 654-672.

Cooper, L. N., Dawson, S. D., Reidenberg, J. S. and Berta, A. (2007b). Neuromuscular anatomy and evolution of the cetacean forelimb. *Anat. Rec. Hoboken* **209**, 1121-1137.

Drucker, E. G. and Lauder, G. V. (1999). Locomotor forces on a swimming fish: three dimensional vortex wake dynamics quantified using digital particle image velocimetry. *J. Exp. Biol.* **202**, 2393-2412.

Ellington, C. P., van den Berg, C., Willmott, A. P. and Thomas, A. L. R. (1996). Leading-edge vortices in insect flight. *Nature* **384**, 626-630.

Fish, F. E. (2002). Balancing requirements for stability and maneuverability in cetaceans. *Integr. Comp. Biol.* **42**, 85-93.

Fish, F. E. (2004). Structure and mechanics of nonpiscine control surfaces. *IEEE J. Ocean. Eng.* **29**, 605-621.

Fish, F. E. and Battle, J. M. (1995). Hydrodynamic design of the humpback whale flipper. *J. Morphol.* **225**, 51-60.

Fish, F. E. and Lauder, G. V. (2006). Passive and active flow control by swimming fishes and mammals. *Annu. Rev. Fluid Mech.* **38**, 193-224.

Goldbogen, J. A., Calambokidis, J., Shadwick, R. E., Oleson, E. M., McDonald, M. A. and Hildebrand, J. A. (2006). Kinematics of diving and lunge-feeding in fin whales. *J. Exp. Biol.* **209**, 1231-1244.

Goldbogen, J. A., Pyenson, N. D. and Shadwick, R. E. (2007). Big gulps require high drag for fin whale lunge feeding. *Mar. Ecol. Prog. Ser.* **349**, 289-301.

Hoerner, S. F. (1965). *Fluid-Dynamic Drag*. Brick Town, NJ: Hoerner Fluid Dynamics.

Hoerner, S. F. and Borst, H. V. (1985). *Fluid-Dynamic Lift*. Bricktown, NJ: Hoerner Fluid Dynamics.

Horwood, J. W. (1990). *Biology and Exploitation of the Minke Whale*. Boca Raton: CRC Press.

Howell, A. (1930). *Aquatic Mammals*. Springfield: Charles C. Thomas.

Kot, B. W. (2005). Rorqual whale surface-feeding strategies: biomechanical aspects of feeding anatomy and exploitation of prey aggregations along tidal fronts. MA Thesis, University of California at Los Angeles, USA.

Küchermann, D. (1953). The distribution of lift over the surface of swept wings. *Aeronaut. Q.* **4**, 261-278.

Lambertsen, R. H. and Hintz, R. J. (2004). Maxillomandibular cam articulation discovered in North Atlantic Minke whale. *J. Mamm.* **85**, 446-452.

Lambertsen, R. H., Ulrich, N. and Straley, J. (1995). Frontomandibular stay of Balaenopteridae: a mechanism for moment recapture during feeding. *J. Mamm.* **76**, 877-899.

Lauder, G. V. (2005). Locomotion. In *The Physiology of Fishes* (3rd edn) (ed. D. H. Evans and J. B. Clairborne), pp. 3-46. Boca Raton: CRC Press.

Lauder, G. V. and Drucker, E. G. (2004). Morphology and experimental hydrodynamics of fish fin control surfaces. *IEEE J. Ocean. Eng.* **29**, 556-571.

Miklosovic, D. S., Murray, M. M., Howle, L. E. and Fish, F. E. (2004). Leading-edge tubercles delay stall on humpback whale (*Megaptera novaeangliae*) flippers. *Phys. Fluids* **16**, L39-L42.

Natural History New Zealand (2002). "Mystery of the Minkes" television documentary. National Geographic Society, 55 min.

Reynolds, O. (1883). An experimental investigation of the circumstances which determine whether the motion of water shall be direct or sinuous, and the law of resistance in parallel channels. *Philos. Trans. R. Soc. Lond.* **174**, 935-982.

Stewart, B. S. and Leatherwood, S. (1985). Minke whale *Balaenoptera acutorostrata* Lacepede, 1804. In *Handbook of Marine Mammals*. Vol. 3 (ed. S. H. Ridgway and R. Harrison), pp. 91-136. London: Academic Press.

van Dam, C. P. (1987). Efficiency characteristics of crescent-shaped wings and caudal fins. *Nature* **325**, 435-437.

Vogel, S. (1994). *Life in Moving Fluids: The Physical Biology of Flow* (2nd edn). Princeton: Princeton University Press.

Woodward, B. L., Winn, J. P. and Fish, F. E. (2006). Morphological specializations of baleen whales associated with hydrodynamic performance and ecological niche. *J. Morphol.* **267**, 1284-1294.